Available online at www.sciencedirect.com
ScienceDirect
Colloids and Surfaces B: Biointerfaces 64 (2008) 22–33
COLLOIDS AND SURFACES B
www.elsevier.com/locate/colsurfb

The lipid-mediated hypothesis of fumonisin B1 toxicodynamics tested in model membranes

Martín G. Theumer [d], Eduardo M. Clop [a], Héctor R. Rubinstein [b,c], María A. Perillo [a,*]

[a] *Bofísica-Química, Depto. Química, Facultad de Ciencias Exactas Físicas y Naturales, Argentina*
[b] *Microbiología de los alimentos, Depto. Bioquím. Clínica, Facultad de Ciencias Químicas, Argentina*
[c] *Instituto Superior de Investigación, Desarrollo y Servicio de Alimentos, Secretaría de Ciencia y Tecnología, Argentina*
[d] *Universidad Nacional de Córdoba, Ciudad Universitaria, Córdoba, Argentina*

Received 22 November 2007; received in revised form 27 December 2007; accepted 3 January 2008
Available online 11 January 2008

Abstract

The disruption of lipidic metabolism was considered a good candidate to explain FB1 toxicity mechanism. In the present work we investigated molecular organizational changes induced by FB1–biomembrane interaction possibly involved in mycotoxic effects.

FB1 was self-aggregated with a critical micellar concentration of 1.97 mM. FB1 (0–81.4 μM), decreased in a dose-dependent manner, the fluorescence anisotropy of TMA-DPH (from 0.349 ± 0.003 to 0.1720 ± 0.0035) in dpPC bilayers, whilst no differences were registered with DPH. At 5.6 μM in the subphase, FB1 increased the lateral surface pressure (π) of a Langmuir film to an extent that depended on the monolayer composition ($\Delta\pi_{\text{dpPC:DOTAP 3:1}} > \Delta\pi_{\text{dpPC:dpPA3:1}} > \Delta\pi_{\text{dpPC}}$), the molecular packing ($\Delta\pi$ decreased linearly as a function of the initial π) and the subphase pH ($\Delta\pi_{\text{pH 2.6}} > \Delta\pi_{\text{pH 7.4}}$ and maximal π allowing the drug penetration $\pi_{\text{cut-off}}$ was 34.3 and 27.7 mN/m at pH 2.63 and 7.4, respectively). FB1 increased the surface potential of dpPC and dpPC:DOTAP monolayers and decreased that of dpPC:dpPA. This suggested that FB1 acquired different orientations and/or foldings depending on the surface electrostatics and the toxin charge state. Moreover, FB1–lipid interactions were transduced into long-range effects at the mesoscopic level affecting the lipidic self-separated lateral domains shape and density.

Keywords: Mycotoxins; Fumonisin B1; Folding; Self-aggregation; Membrane-binding interfacial localization

1. Introduction

The fungal secondary metabolism produces, by means of a few common biosynthetic pathways, a wide spectrum of chemically diverse low-molecular weight molecules, many of them exhibiting potent biological activities [1,2]. Those that induce toxic responses in humans and animals are called mycotoxins, a special class of secondary metabolites synthesized by toxigenic fungal stocks. The fumonisins are mycotoxins produced by environmental moulds of the genus *Fusarium*. This group of toxins, currently divided into the A, B, C, and P series, includes at least 28 analogues formed by a 20-carbon aliphatic chain, resembling the chemical structure of sphingosine [3]. Recent studies led to the identification of new fumonisin stereoisomers, increasing the number of chemically different compounds within the group [4]. Fumonisin B1 (FB1) (Fig. 1), mainly produced by toxigenic stocks of *F. verticillioides* (Sacc.) Niremberg (e.g. *F. moniliforme* Sheldon) and *F. proliferatum* (Matsushima) Niremberg [5], has the major impact in human and animal health and is

Abbreviations: BTB, bromothymol blue (3′,3″-dibromthymolsulfonephthalein); CMC, critical micellar concentration; DPH, 1,6-diphenyl-1,3,5-hexatriene; dpPA, 1,2-dipalmitoyl-*sn*-glycero-3-phosphate; dpPC, 1,2-dipalmitoyl-*sn*-glycero-3-phosphocholine; DOTAP, 1,2-dioleoyl-3-trimethylammonium-propane (chloride salt); EPC, L-α-phosphatidylcholine (egg, chicken-99%); FB1, fumonisin B1; MER, merocyanine 540 (5-[(sulfonyl-2(3*H*)-benzoxazoylidine)-2-butenyldene]-1,2-dibutyl-2-thiobarbituric acid); MLV, multilamellar vesicles; NBD-PE, 1,2-dipalmitoyl-*sn*-glycero-3-phosphoethanolamine-*N*-(7-nitro-2-1,3-benzoxadiazol-4-yl) (ammonium salt); TMA-DPH, *N*,*N*,*N*-trimethyl-4-(6-phenyl-1,3,5-hexatrien-1-yl)phenylammonium *p*-toluenesulfonate.

* Corresponding author at: Bofísica-Química, Cátedra de Química Biológica, Depto. Química, Fac. Cs. Ex., Fís. y Nat., Universidad Nacional de Córdoba, Av. Vélez Sarsfield 1611, X5016GCA Córdoba, Argentina.
Tel.: +54 351 434 4983x5; fax: +54 351 433 4139.
E-mail address: mperillo@efn.uncor.edu (M.A. Perillo).

0927-7765/$ – see front matter © 2008 Elsevier B.V. All rights reserved.
doi:10.1016/j.colsurfb.2008.01.002

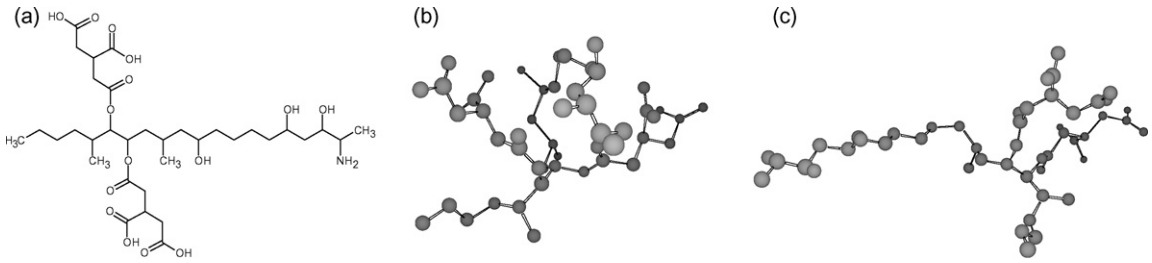

Fig. 1. FB1 chemical structure and theoretically derived molecular geometries: (a) chemical structure of FB1; (b) a compact-amphipathic minimum energy conformation in vacuum determined by semi-empirical quantum mechanics calculations (present work); (c) extended-zwitterionic structure such as that predicted by molecular dynamics simulations in water [34].

also the fumonisin most frequently found in feedstuffs destined for human and animal consumption.

Higher incidences of severe pathologies in humans, such as primary hepatocellular carcinoma [6], esophageal cancer [7–9], and neural tube defects [10], were found in populations chronically exposed to diets contaminated with FB1. However, neither an illness–exposure relationship nor the mechanisms involved in the toxicity of this mycotoxin were clearly established yet. Some pathological changes appear to be a consequence of the immunotoxic action of FB1, which was observed in several experimental models in animals [11,12]. On the other hand, the direct genotoxic action and the cell oxidative stress induced by FB1, among others, were suggested as probable mechanisms that could be involved in its toxicity in animal cells [13,14]. FB1 enhanced the production of free radicals and then accelerated the lipid peroxidation-associated chain reactions, this being a potential mechanism which can increase the oxidative stress and the cellular damage [15].

The competitive inhibition of ceramide synthase (CS), and the resultant disruption of sphingolipids metabolism, is believed to be the main mechanism of FB1 toxicity [16]. This inhibition was considered independent of the membrane environment because, *in vitro*, it was observed not only with the membrane bound but also with a yeast-purified CS [17]. However, in all the conditions tested, this enzyme was embedded inside an anisotropic matrix represented either by the lipidic bilayer membrane or by a detergent micelle ("purified" CS). Hence, similar to what happened with many lipolytic enzymes like phospholipases [18] as well as with enzymes associated with sphingolipids metabolism (e.g. neuraminidase [19], and sphingomielinase [20]), CS might be modulated by the interfacial reorganization of either its amphipathic substrates and/or its own molecular environment. Therefore, the inhibitory effect of FB1 on CS activity as well as the sphingolipid metabolism disruption induced by FB1 might not be a typical enzyme–inhibitor type direct interaction but a consequence of mycotoxin-induced changes in the dynamic organization of the lipid phase.

The lipid-based mechanism involving inhibition of CS as the initial stages of FB1 action appears to be a key step in the toxicology of fumonisins, but there is some evidence that the FB1 toxicity is not solely due to this enzymatic inhibition [21]. Some of the toxic effects of FB1 may be related with modifications in the lipidic composition and functionality of cell membranes, which in turn could modulate the biological activity of membrane-associated proteins [22,23]. It was shown that FB1 enhanced the normal membrane fluidity in a macrophage cell line exposed 24 h to the toxin, which was explained by alterations in the sphingolipids metabolism and lipid peroxidation [24]. Thus, FB1 modifies the plasma membrane biological properties by means of an indirect effect, inducing changes in its phospholipid composition. In addition, a study on the effects of FB1 on the structural and dynamic properties of dpPC multilamellar vesicles (MLV) showed that FB1 increased the fluidity of fluid-phase membranes, and it increased the rigidity of membranes in the gel phase. Also, the results of these experiments suggest that the FB1 tricarballylic acid moieties mimic the structure of the sphingolipids polar groups [25].

Beyond the above-mentioned evidences, the knowledge of the early events that trigger FB1 action mechanism is scarce, particularly the information related with the mycotoxin accessibility to the membrane environment. Biophysical approaches in systems of defined composition and organization have been shown to be able to provide useful information on these topics [26–29]. Hence, the aim of the present work was to study the FB1 self-assembling ability, surface activity and localization within the membrane structure, as well as the physico-chemical properties of the lipid–water interface that allow FB1 adsorption and penetration.

2. Materials and methods

2.1. Materials

FB1 of analytical standard (purity >95%) was provided by Programme on Mycotoxins and Experimental Carcinogenesis (PROMEC, Republic of South Africa). Phospholipids and NBD-PE were from Avanti Polar Lipids (Alabaster, AL, USA). BTB, DPH and TMA-DPH were from Sigma Co. (St. Louis, MA, USA). MER was from ICN (Aurora, OH, USA). Other drugs and solvents were of analytical grade.

2.2. Quantification of FB1

The FB1 crystals were dissolved in ethanol. FB1 was quantified in samples of this solution conveniently diluted with acetonitrile:water (1:1, v/v), as described previously [30]. An aliquot (50 μL) of the diluted solution was derivatised with 200 μL of an *o*-phthaldialdehyde solution, obtained by

adding 5 mL of 0.1 M sodium tetraborate and 50 μL of 2-mercaptoethanol to 1 mL of methanol containing 40 mg of *o*-phthaldialdehyde. The mycotoxin was detected and quantified with a Hewlett Packard HPLC equipped with a fluorescence detector. The wavelengths used were 335 and 440 nm for excitation and emission of fluorescence, respectively. An analytical reverse-phase C_{18} column (150-mm length by 4.6-mm internal diameter and 5-μm particle size), connected to a C_{18} precolumn (20 mm × 4.6 mm; 5-μm particle size), was used. The mobile phase was methanol:0.1 M NaH_2PO_4 at a 3:1 ratio (v/v); the pH was set at 3.35 ± 0.2 with orthophosphoric acid, and a flow rate of 1.5 mL/min was used. The quantification of FB1 was carried out by comparing the peak areas obtained for the ethanolic solution of FB1 to those corresponding to standards (purity >95%) of 10.5, 5.25 and 2.63 μg FB1 per mL (PROMEC, Republic of South Africa).

2.3. Determination of critical micellar concentration (CMC)

The CMC value of FB1 was determined by dispersing it in water, at different final concentrations (between 0 and 2.98 mM), in the presence of the hydrophobic dye bromothymol blue (BTB) (80 μM final concentration). The samples were incubated at room temperature during 10 min and then the absorbance was measured at 432 nm with a Beckman DU 7500 spectrophotometer. The absorbance values were plotted against the concentration of FB1 (mM), and then the mycotoxin CMC was determined by intersection of the regression lines for A_{432} *vs.* [FB1] in the plane regions of the curve (ranges 0.32–1.73 and 2.18–2.98 mM of FB1).

2.4. Penetration of FB1 in lipid monomolecular layers at the air–water interface

Phospholipid monomolecular layers at the air–water interface were prepared and monitored as described previously [29,31] using a Minitrough II from KSV Instruments Ltd. (Helsinki, Finland). Chloroform solutions (5–30 μL) of the lipids (EPC, dpPC, dpPC:dpPA 3:1, or dpPC:DOTAP 3:1) were spread on the surface of the aqueous solution contained in a circular Teflon trough (4.5-cm diameter and 0.5-cm depth). After 5 min, to allow the evaporation of chloroform, the lateral surface pressure (π) was measured by the Wilhelmy plate method. Reproducibility of the π values was ±0.001 mN/m. The subphase (8.5 mL, 15.9 cm^2 of surface area) was under continuous stirring with a miniature Teflon-coated rod spinning at 150–250 rpm.

FB1 penetration in the monolayer was evaluated at different monolayer compositions (a), molecular packings (b) and mycotoxin concentration in the subphase (c).

(a) *The effect of monolayer composition*: The penetration of FB1 in the monolayer was studied at a constant initial surface pressure ($\pi_i \approx 10$ mN/m), 7 μL of an ethanolic solution of FB1 was injected in the subphase (bidistilled water) under monolayers of dpPC, dpPC:dpPA 3:1, or dpPC:DOTAP 3:1, at 5.65 μM FB1 final concentration. Then, π was recorded as a function of time (t). The experiment was performed by triplicate for each monolayer composition, and the $\Delta\pi_{max}$ values were determined from the difference between π_{max} (reached at the plateau at $t = 8$ min) and π_i (at $t = 0$ min). The capacity of FB1 to stabilize at a free air–water interface was also investigated by following a similar procedure but in the absence of monolayer.

(b) *The effect of the molecular packing*: EPC monolayers were set at different π_i (5.5–24 mN/m) and FB1 (ethanolic solution, 9 μL) was injected in the subphase composed of Tris–HCl buffer (100 mM, pH 7.4) or citrate (100 mM, pH 2.63), at a final FB1 concentration of 7.87 μM (5.68 μg/mL). After the injection of FB1, the temporal dependence of π_t was recorded. The values of $\Delta\pi_{max}$ were plotted against π_i. A straight-line equation was fitted and its intersection with the abscise axis gave the maximum π allowing FB1 penetration ($\pi_{cut\text{-}off}$) at different subphase pH. The ordinate ($\Delta\pi_0$) was taken as a measure of FB1 efficacy to induce the expansion of the monolayer. Control experiments were run similarly, by injecting ethanol (FB1 vehicle) in the subphase.

(c) *The effect of FB1 concentration in the subphase*: FB1 penetration in monolayers of EPC packed at $\pi_i \approx 10$ mN/m was measured as a function of time. FB1 concentration in the subphase (bidistilled water) varied between 0 and 80 μM.

The rate constants for the adsorption and desorption processes at the monolayer–water interface were determined from a plot of $\Delta\pi_t = \pi_t - \pi_i$, *vs.* t (the time elapsed after the drug injection in the subphase) analyzed on the basis of a single-exponential model represented by the following equation:

$$\Delta\pi_t \cong \left[1 - \exp\left(-\frac{t}{\tau}\right)\right] \quad (1)$$

and the time constant (τ) values could be determined for each individual FB1 concentration in the subphase. Then, the rate constants for the adsorption (k_a) and desorption (k_d) processes were obtained by fitting Eq. (2) to the plots of $1/\tau$ *vs.* drug concentration.

$$\frac{1}{\tau} = k_d + k_a[\text{drug}] \quad (2)$$

Finally, Eq. (3) allowed calculation of the association-binding constant (K_b) [29,32], as follows:

$$K_b = \frac{k_a}{k_d} \quad (3)$$

2.5. Surface pressure–area and surface potential–area isotherms

For the π–molecular area isotherms, π values were measured at different molecular areas of the pure lipid (dpPC, dpPC:dpPA 3:1, or dpPC:DOTAP 3:1) containing or not 10 mol% of FB1. For these experiments we used a rectangular trough fitted with two barriers that were moved synchronously by an electronic switching. The signal corresponding to the surface area (automatically determined by the KSV Minitrough from KSV

Instruments, Helsinki, Finland) according to the relative position of the two compression barriers, the output from the surface pressure (π) transducer (measured automatically by the Minitrough with a platinized Pt foil 5-mm wide × 20-mm long × 0.025-mm thick), and the surface potential (ΔV) registered by the voltage-measuring system (vibrating plate method; KSV Instruments, Helsinki, Finland) were fed into a personal computer through a serial interface using a specific software. Before each experiment the trough was rinsed and wiped with 70% ethanol and several times with bidistilled water. The absence of surface-active compounds in the pure solvents and in the subphase solution (bidistilled water) was checked before each run by reducing the available surface area to less than 10% of its original value after enough time was allowed for the adsorption of possible impurities that might have been present in trace amounts. The monolayer was compressed at a constant low rate of 20 mm^2/s at 28 ± 0.5 °C. A lower compression rate (12 mm^2/s) was tested, and identical results were obtained.

2.6. Epifluorescence microscopy of monolayers

Monolayers containing dpPC were doped with 1 mol% NBD-PE and observed with an inverted epifluorescence microscope. Briefly, a KSV Minisystems surface barostat was mounted on the stage of a Nikon Eclipse TE2000-U (Tokyo, Japan) microscope, which was supplied with 20× long-working distance optics. The Teflon trough used had a 35-mm diameter quartz window at its base, which allowed the observation of the monolayer through the trough. The monolayer morphology was documented with a color video camera Nikon DS-5M with a supported resolution up to 2560–1920 pix (Capture). FB1 (0.37 μM final concentration) was injected in the subphase (500 mM NaCl). Experiments were performed either at constant π (15 or 35 mN/m) by applying an automatic continuous π-compensation mechanism that allowed the area expansion upon FB1 penetration, or at constant area and varying π (typical penetration experiment). Images were taken at different times after FB1 injection in the subphase. Then, the percentage of total film area contributed by domains in liquid-expanded phase (brigh fluorescent areas) was calculated by analyzing the pictures with Adobe Photoshop 7.0 software (USA).

2.7. Preparation of multilamellar vesicles

The appropriate amounts of dpPC dissolved in chloroform was placed in a glass tube and evaporated thoroughly at 50 °C. Multilamellar vesicles were prepared by hydration of the lipid film with bidistilled water, intensive vortexing and heating at 50 °C. The final dpPC concentration was 41 μM (0.03 mg/mL). The absorbance of the MLV suspension was ≤0.05 in the 300–600 nm wavelength range.

2.8. Steady-state fluorescence

The fluorescent probes DPH (2 μM) and TMA-DPH (6 μM) were added to the dpPC MLV suspension prepared as described above and incubated for 1 h at room temperature. The effects of FB1 (0-81.4 μM) on the DPH and TMA–DPH steady-state fluorescence anisotropy were studied. Anisotropy values were calculated from the emission fluorescence intensities (F) at λ_{em} = 430 nm (λ_{ex} = 356 nm) measured with the excitation and the sample polarizer filters oriented parallel ($F_{||}$) and perpendicularly ($F_{\perp}$) one with respect to the other, in a L-format FluoroMax-3 spectrofluorometer (Jovin Yvon, Horiba). Slits width and integration time were set at 2 nm and 15 s, respectively. The final percentage of ethanol (FB1 vehicle) incorporated to the MLV suspension was 1.18%. Steady-state fluorescence anisotropy (A) was calculated as

$$A = \frac{I_{VV} - I_{VH}G}{I_{VV} + 2I_{VH}G}, \quad G = \frac{I_{HV}}{I_{HH}} \tag{4}$$

where I_{VV}, I_{HH}, I_{VH} and I_{HV} are the values of the different measurements of fluorescence intensity taken with both polarizers in vertical (VV) and horizontal (HH) orientations or with excitation polarizer vertical and emission polarizer horizontal (VH) or *vice versa* (HV). G is a correction factor for differences in sensitivity of the detection system for vertically and horizontally polarized light [33]. Anisotropy values were plotted against [FB1] (μM).

2.9. Computation of molecular parameters

The software used to design the starting point molecules was Alchemy III. Energy minimization in vacuum was performed with the CS Chem3D 3.5.1 modified version of Allinger's MM2 Force Field and semi-empirical quantum mechanics calculation of dipole moments and solvation area in water was done with the MOPAC 3.5.1 module with MNDO potential function (Cambridge Soft Corporation, MA, USA).

2.10. Statistical analysis

Data from these studies were analyzed by two-tailed ANOVA. Results giving p values ≤0.05 were considered significantly different, and further analyzed by the Tukey–Kramer post hoc test. Differences between groups were considered statistically different for p values ≤0.05.

3. Results

3.1. FB1 molecular properties and self-assembly

The chemical structure of FB1 is depicted in Fig. 1a. In its lowest energy conformation in the vacuum (Fig. 1b) it exhibited a strong dipole moment (4.677 Debye) and a solvation area in water (VDW) of 303.86 $Å^2$ as determined from semi-empirical quantum mechanics calculations. The conformation leading to the lowest dipole in vacuum (Fig. 1c) was similar to that obtained by others from dynamic simulation in water [34].

In order to investigate the self-assembling of FB1, changes in the absorbance of BTB were evaluated as a function of the mycotoxin concentration. The results, depicted in Fig. 2, showed that FB1 induced a biphasic decrease in BTB absorbance at

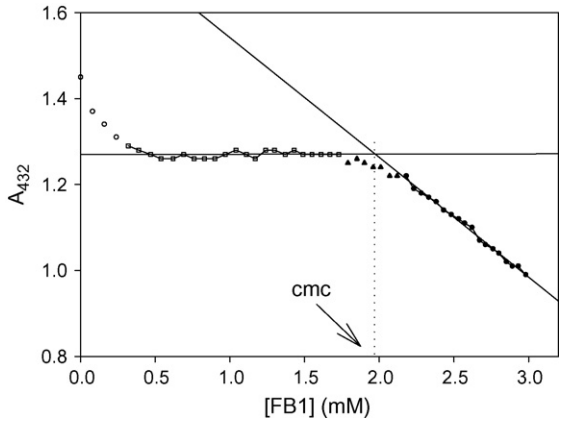

Fig. 2. FB1 self-assembly in aqueous medium. Absorbance measurements (A) of BTB at 432 nm as a function of the FB1 concentration (mM). The CMC value (pointed to by the arrow) was determined from the intersection of regression lines for A *vs.* [FB1] within the ranges 0.32–1.73 and 2.18–2.98 mM of FB1.

432 nm (A_{432}). Ethanol (FB1 vehicle) did not affect A_{432} (not shown). The FB1 c.m.c. value resulted 1.97 mM and was determined from the intersection between the two asymptote lines as indicated in Fig. 2.

3.2. Effects of FB1 in the fluorescence anisotropy of DPH and TMA-DPH

Anisotropy values for DPH and TMA-DPH in dpPC MLVs were evaluated in the presence of different FB1 concentrations (0–81.4 μM). The results of these experiments are depicted in Fig. 3. Similar fluorescence anisotropy values of DPH and TMA-DPH (0.35 ± 0.01 and 0.349 ± 0.003, respectively) were observed in MLVs in the absence of FB1. A dose-dependent decrease in the anisotropy of TMA-DPH fluorescence (from 0.349 ± 0.003 to 0.1720 ± 0.0035) was observed when FB1 was added to the vesicle suspension, whilst no differences were registered in the DPH steady-state fluorescence anisotropy (from 0.35 ± 0.01 to 0.351 ± 0.002), within the FB1 concentrations studied.

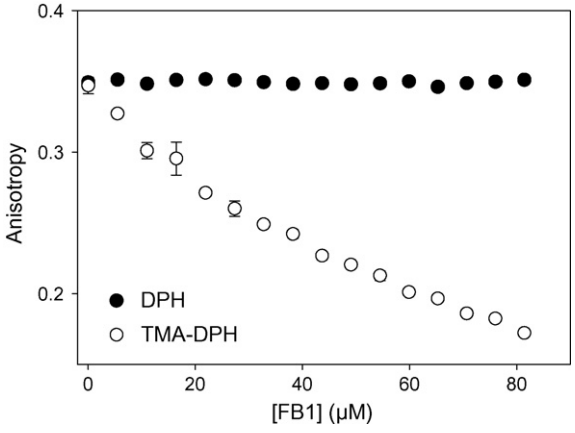

Fig. 3. Effect of the FB1 concentration on the fluorescence anisotropy of DPH and TMA-DPH in dpPC multilamellar vesicles (MLVs).

3.3. Penetration in phospholipids monomolecular layers at the air–water interface

The increase in surface pressure elicited by the association on the mycotoxin to previously formed lipid monolayers can be employed as a measure of the FB1 ability to interact with organized lipids. In the presence of FB1 in the subphase under EPC monolayers, at all the concentrations (Fig. 4a and b) and π_i (Fig. 4c) studied, π firstly increased hyperbolically (Fig. 4b), after reaching a maximum it suffered an exponential decrease and finally it reached a plateau (Fig. 4a and c). At $t = 8$ min this plateau, representing the FB1 partition equilibrium state, was already established so, $\Delta\pi_{max}$ was calculated as the difference between $\pi_{8\ min}$ and π_i.

3.3.1. Effect of FB1 concentration in the subphase

The penetration of FB1 in EPC monolayers was a concentration-dependent process (Fig. 4a). The value of $\Delta\pi_{max}$ increased with FB1 concentration with a limiting slope 0.050 mN/m μM^{-1} (0.036 mN/m μL^{-1} sample volume) (Fig. 4d). Although the addition of EtOH alone, in amounts equivalent to those applied in the FB1 containing samples, also increased $\Delta\pi_{max}$, its effect was significantly lower than that observed with FB1 (slope 0.019 mN/m μL^{-1} EtOH) (Fig. 4d). The kinetics of the initial drug binding (Eq. (1) applied to $\Delta\pi$ *vs.* time plots) allowed the determination of the τ values at different FB1 concentrations (Fig. 4e) and by the fitting of Eq. (2) the rate constants for the association and dissociation process could be determined ($k_a = 6.4 \times 10^4\ min^{-1}\ M^{-1}$; $k_d = 8.225\ min^{-1}$) and the thermodynamic association constant ($K_d = 7.8 \times 10^{-5}\ M^{-1}$) was calculated (Eq. (3)).

3.3.2. Effect of the initial surface pressure

At a constant subphase concentration of FB1 (8 μM), the value of $\Delta\pi_{max}$ decreased linearly as a function of the molecular packing of the zwitterionic monolayer (EPC), represented by the π_i value (Fig. 4c). Penetration was more efficient from the acidic subphase of citrate (pH 2.63) compared with the neutral subphase of Tris–HCl buffer (pH 7.4) (Fig. 4f). This was evidenced by the steeper $slope_{2.63} = -0.367$ mN/m $(mN/m)^{-1}$ and $\pi_{cut\text{-}off,\ 2.63} = 34.3$ mN/m of the former compared with the later ($slope_{7.4} = -0.101$ mN/m $(mN/m)^{-1}$ and $\pi_{cut\text{-}off,\ 7.4} = 27.7$ mN/m).

3.3.3. Effect of the monolayer composition

These results were depicted in Fig. 5. The injection of FB1, at a concentration below its c.m.c., in the subphase under a zwitterionic (dpPC), negatively (dpPC:dpPA) or positively charged (dpPC:DOTAP) monolayers initially packed at 10 mN/m, the following maximal increase in surface pressures were detected: $\Delta\pi_{max}$ of 7.02 ± 0.38 mN/m, 8.83 ± 0.52 mN/m and 10.18 ± 0.44 mN/m, respectively (Fig. 5). The penetration of FB1 was significantly higher in the dpPC:dpPA ($p \leq 0.01$) and dpPC:DOTAP ($p \leq 0.001$) interphases, with respect to dpPC. Besides, the FB1 penetration was higher in dpPC:DOTAP than the observed in dpPC:dpPA ($p \leq 0.05$).

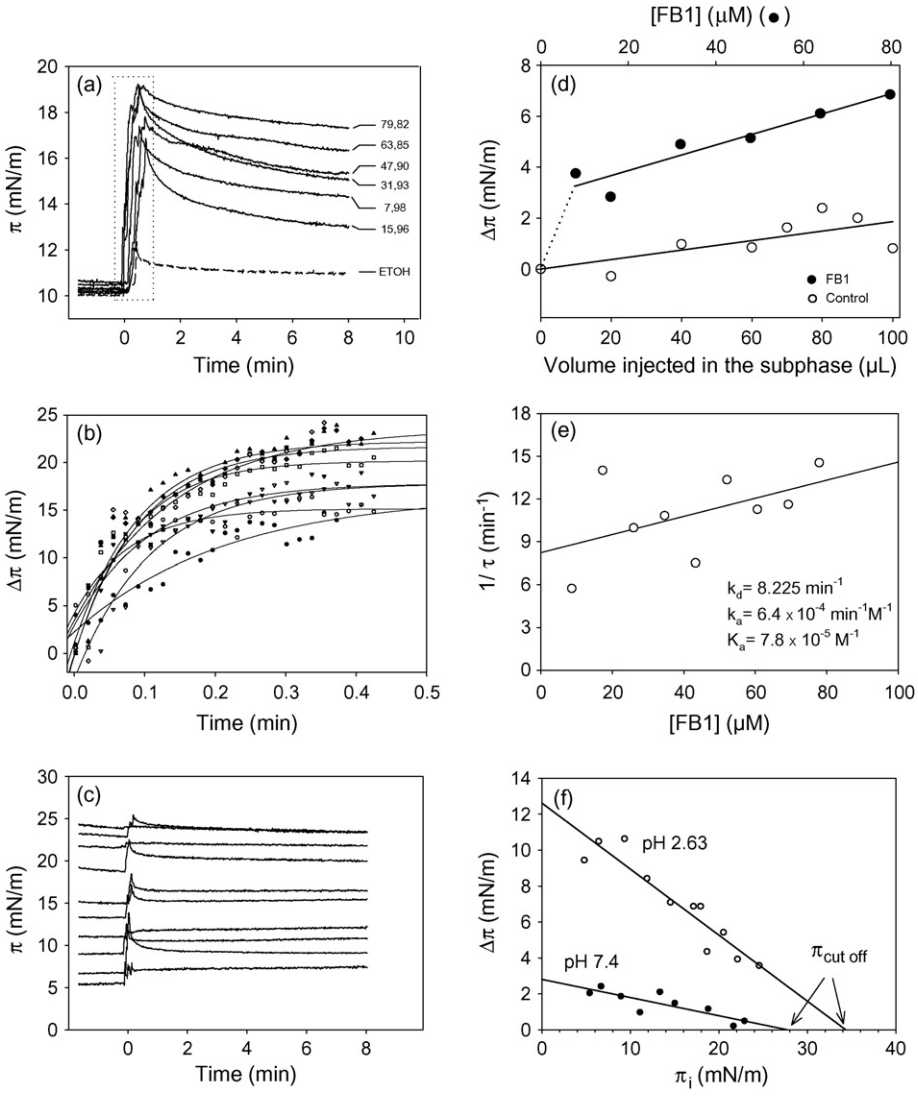

Fig. 4. FB1 penetration in EPC monolayers. (a) At constant $\pi_i \approx 10.3$ mN/m and varying FB1 subphase concentration; 0 μM FB1 correspond to 100 μL ethanol used as the mycotoxin vehicle; subphase: bidistilled water. (b) Initial penetration kinetics: enlargement of the area enclosed in the dotted lined box shown in panel (a). (c) FB1 penetration at different π_i and 7.9 μM fixed final concentration in a Tris (100 mM, pH 7.4) buffer subphase. (d) $\Delta\pi = \pi_{8\,min} - \pi_i$ were determined from data shown in panel (a). (e) Firstly, τ values were calculated by fitting Eq. (1) to each of the curves shown in panel c; then $1/\tau$ *vs.* FB1 concentration plots were submitted to a linear regression analysis to determine the kinetic and thermodynamic constants according to Eq. (2). (f) $\Delta\pi = \pi_{8min} - \pi_i$ data taken from experiments such as that shown in panel b; numbers indicate the subphase pH obtained with 10 mM Tris pH 7.4 or 100 mM citrate pH 2.63 in each subphase. The $\pi_{cut\text{-}off}$ values are pointed to by the arrows.

The incorporation of FB1 to a clean air–water interface, in the absence of a lipid monolayer at the interface, induced a $\Delta\pi_{max} = 8.2$ mN/m. However, the pure FB1 monolayer so formed, could not remain stable under compression (not shown).

3.4. Surface pressure–area and surface potential–area isotherms of FB1–lipid mixed monolayers

Fig. 6a shows that π-area isotherm of the mixed FB1–dpPC monolayer exhibited an expansion along the whole surface pressure range (from zero to collapse) and a decrease in the cooperativity of the bi-dimensional phase transition with respect to pure dpPC. The mean molecular area of the FB1–dpPC mixture (42 Å^2) was slightly higher than the minimum molecular area of pure dpPC (41 Å^2). The collapse pressure, hence the monolayer stability, also increased in the presence of FB1 (π_{cdpPC} 53 mN/m < $\pi_{c,\,FB1\text{–}dpPC}$ = 60 mN/m).

When present in mixtures with dpPC:dpPA (Fig. 6b) and dpPC:DOTAP (Fig. 6c) monolayers, FB1 induced an increase in the mean molecular area at low pressures. This monolayer expansion became lower upon compression and in the case of the mixture containing DOTAP the minimum molecular area resulted lower in the presence of FB1 if compared with its absence ($A_{min\ dpPC:DOTAP} = 32$ Å^2/molec and $A_{min\ dpPC:DOTAP\ FB1} = 29$ Å^2/molec). FB1 decreased the collapse pressure of the mixture containing dpPA (from $\pi_{c\ PC:PA} = 63$ mN/m in its absence to $\pi_{c\ PC:PA\ FB1} = 58$ mN/m in its presence) but not that of the dpPC:DOTAP mixture.

Fig. 6 shows that the ΔV increased upon monolayer compression. Surface potential values followed the expected order

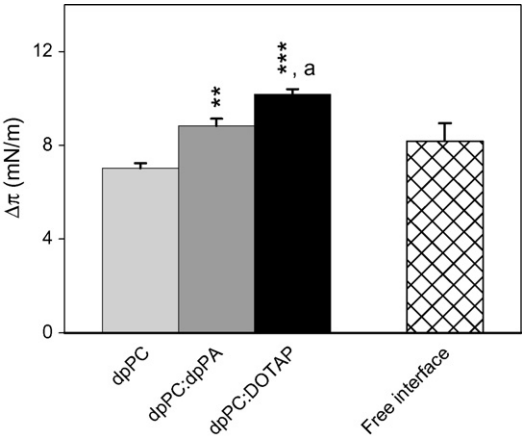

Fig. 5. Effect of the interface chemical composition on the FB1 interfacial penetration. FB1 was injected in either the aqueous phase of a free air–water interface ($\pi_i = 0$ mN/m) (pattern bar) or in the subphase under dpPC (light grey bar), dpPC:dpPA (3:1) (dark grey bar), or dpPC:DOTAP (3:1) (black bar) monolayers set at a constant initial surface pressure ($\pi_i \approx 10$ mN/m). The $\Delta\pi = [\pi_{max} - \pi_i]$ values were evaluated, where π_{max} was the π reached at $t = 8$ min. and π_i was π at $t = 0$ min. FB1 (7 μL ethanolic solution) was injected in the subphase (bidistilled water pH 4.86) to obtain a 5.65 μM final concentration. Bars represent the mean ± S.E.M. of independent triplicates. $^{**}p \leq 0.01$ (dpPC:dpPA *vs.* dpPC); $^{***}p \leq 0.001$ (dpPC:DOTAP *vs.* dpPC); $^{a}p \leq 0.05$ (dpPC:DOTAP *vs.* dpPC:dpPA).

for negatively < zwitterionic < positively charged monolayers in the absence of FB1. If compared with pure lipid monolayers, the whole $\Delta V - A$ isotherm obtained with FB1–lipid mixed monolayers was displaced either upwards, when the lipid were the zwitterionic dpPC or the negatively charged dpPC–dpPA mixture, or downwards in the case of mixtures containing the positively charged DOTAP. This strongly suggests a different orientation of the resultant FB1 molecular dipole in the former monolayers if compared with the latter.

3.5. Lateral domains expansion and coalescence induced by FB1 penetration in dpPC monolayer

Before the injection of FB1 in the subphase, the enantiomeric dpPC monolayers at 15 mN/m (Fig. 7a) showed the typical elongated armed triskelion structures with curvatures in the arms. Domains deformation and coalescence are observed at higher surface pressures. As shown in Fig. 7 (left and central panels) at constant $\pi = 15$ mN/m as well as 35 mN/m, the FB1 binding to the monolayer induced an expansion of condensed phase domains maintaining almost unchanged the domain shape. On the other hand, when experiments were performed at constant area and the π increase upon FB1 penetration was allowed (left panel), domains coalescence were observed which, at long times, led to a continuous condensed phase. A quantitative analysis is shown in Fig. 8.

4. Discussion

In the present work we provide experimental evidence that may help to understand FB1 toxicological action mechanisms at

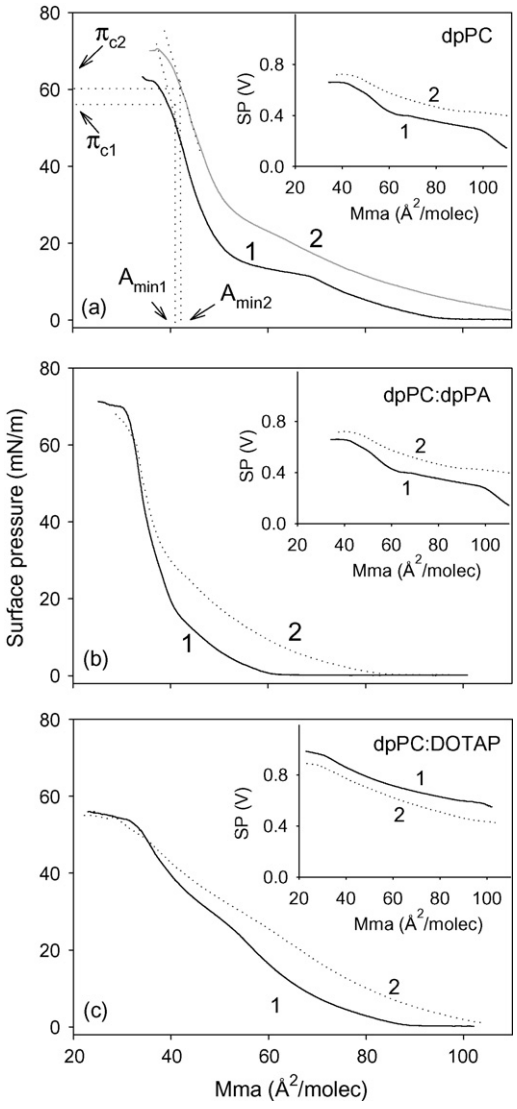

Fig. 6. Effects of FB1 in the surface pressure–area and surface potential–area compression isotherms. (a) dpPC, (b) dpPC–dpPA 3:1 mol/mol and (c) dpPC–DOTAP 3:1 mol/mol. Monolayers were prepared by dispersing the lipids (1) or a lipid–FB1 9/1 mol/mol pre-mixture (2), on the water surface. SP: surface pressure; Mma: mean molecular area. In (a) dotted straight lines indicate the determination of the collapse point and the values of its defining variables, the minimum molecular area A_{min} and the collapse pressure π_c, which are pointed to by the arrows.

the early stages of its interaction with biomembranes. We evaluated the toxin molecular conformational and self-organizing properties, the characteristics of the initial membrane state that controls the toxin–membrane interaction and the changes in the membrane organization triggered by the toxin binding and penetration.

4.1. FB1 molecular conformations and self-assembled structures

Keeping in mind the molecular structure and possible conformations adopted by FB1 in vacuum and in water (Fig. 1) may contribute to the interpretation of the results presented in the present paper.

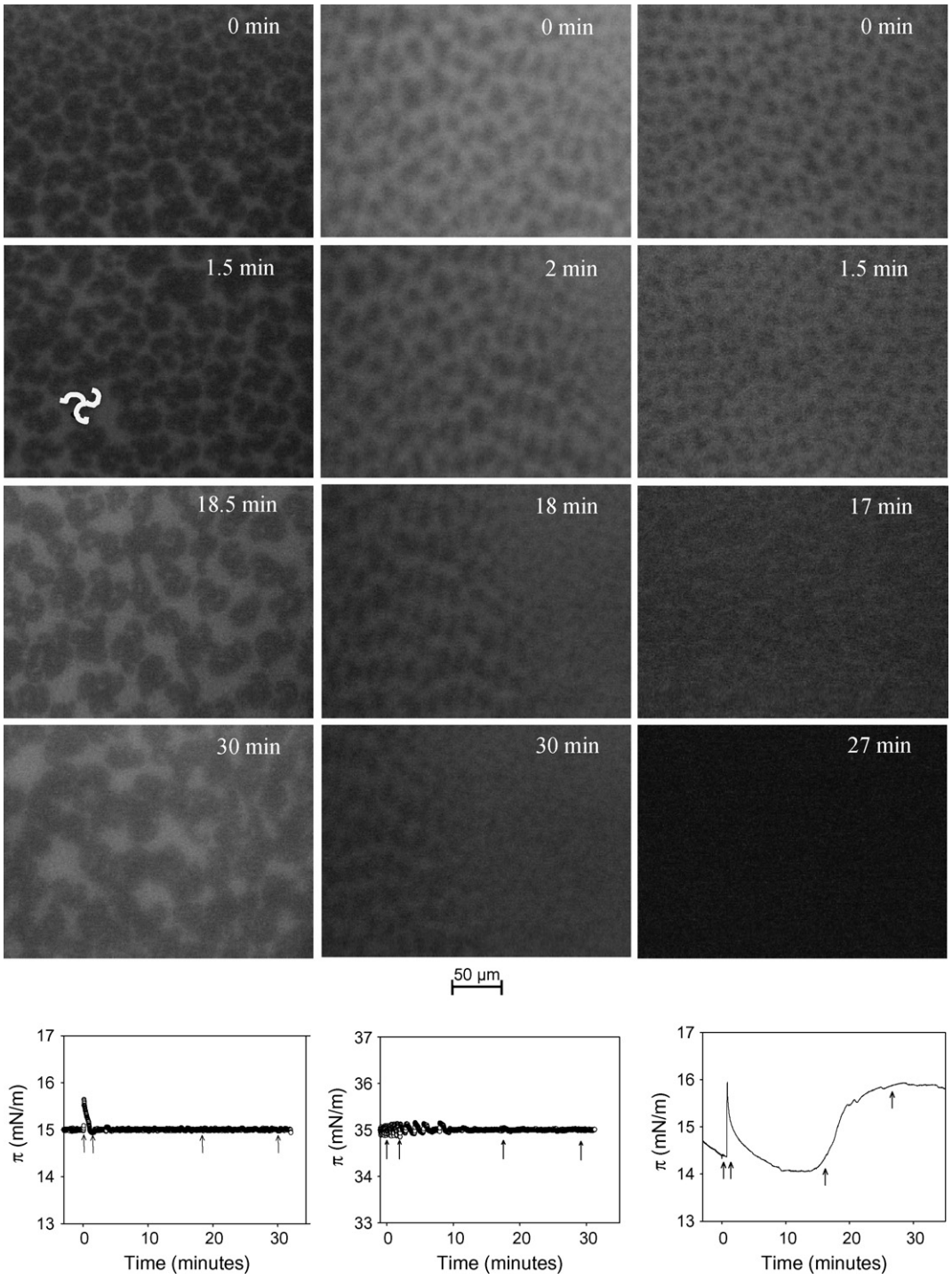

Fig. 7. Growth of condensed phase domains in pure dpPC monolayers upon FB1 penetration. dpPC monolayers were doped with 1 mol% NBD-PE. Images were taken at the designated points in the temporal profiles shown at the bottom. Before the FB1 injection, the monolayer was set at an initial $\pi_i = 15$ mN/m (left panels) or 35 mN/m (central panel) remaining constant through an area compensation, or at 15 mN/m but varying freely at constant surface area (right panels). A typical triskelion structure is remarked in one of the panels intending to serve as a look guide.

4.1.1. FB1 conformations

The high dipole moment determined from the minimum energy state in vacuum would be due to the big polar head formed by three chains, two of them containing two carboxylic groups each and several hydroxyls and the opposite end represented by a short hydrocarbon chain (Fig. 1b). These conclusions are consistent with the molecular mechanics calculated structures reported by Beier et al. which was described as a unique folding that resembled that of a folded peptide with a cage-like structure formed by the folding of the amine backbone with the two esterified trimethylpropane-1,2,3-tricarboxylic acid side chains [35]. The three-dimensional structure formed was compared with the claw of a bird. This cage-like structure brought the amine, hydroxyls, and carboxylic acid groups into close prox-

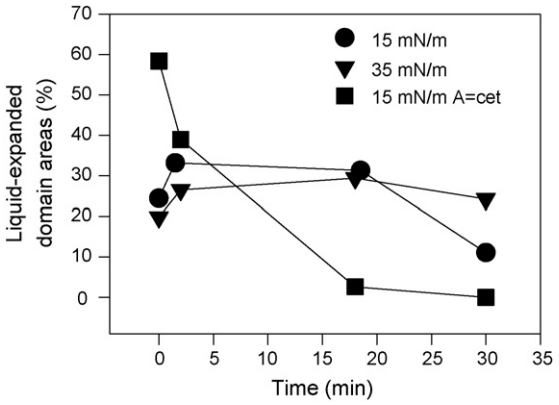

Fig. 8. Percentage of total film area contributed by liquid-expanded phase domains upon FB1 penetration in dpPC monolayers.

imity. The electrostatic potential surfaces showed that most of the exposed surfaces of these molecules were hydrophobic in nature [36]. It may be argued that because these low-energy conformations were found in vacuum conditions they are biased by the uncharged state of the molecule and the lack of competing interactions with water.

On the other hand, the minimum dipole conformation in vacuum (Fig. 1c, present work) was similar to that obtained by Momany and Dombrink-Kurtzman (2001) from molecular dynamics simulations performed in water [34]. In this case FB1 can be described as a long zwitterionic-like molecule with a basic group at one end of the chain and four charged carboxyl groups a the other branched ends. A simulation reproducing a dilute solution showed the possibility of a molecular dimer formation. This may energetically drive the preferred conformation to an extended form. Despite the vacuum state was considered most probably responsible for the compact structure, a transient conformation of only a few picoseconds appeared in the molecular dynamics simulations in which the amine to tricarballiylic acid distance was very short for both tricarballylic acid groups [34].

4.1.2. Self-assembly and possible structures formed

Upon FB1 self-aggregation, a compartment with a polarity markedly different from that of water would appear. The partitioning of BTB in this hydrophobic and anisotropic environment would lead to a decrease in A_{432} [27]. This was demonstrated in Fig. 2. The initial decrease in the absorbance of BTB, within the range 0–0.47 mM FB1, can be ascribed to the continuous pH change induced by the addition of FB1 ($pK_{a,-COO-} \approx 4.19$–$5.48$) which dissolved in water in the monomeric form and affected the acid base equilibrium of BTB ($pK_{a,\,BTB} \approx 7.3$). Subsequent pH changes due to FB1 addition (from 0.47 to 3 mM) would be unable to induce further changes in BTB equilibrium and this may explain the constancy in the BTB absorbance at 432 nm within the range 0.47 and 1.97 mM FB1 (the left edge was determined from the intersection between the two asymptote lines indicated in Fig. 2). Above 1.97 mM the FB1 absorbance *vs*. FB1 concentration plot exhibited an abrupt slope change from zero to negative values. This behavior can be explained by the amphiphilic nature of FB1 which self-aggregated in water when it reached the critical micellar concentration value (c.m.c. = 1.97 mM) and allowed the appearance of a hydrophobic environment where BTB partitioned.

The type of the self-assembled structures formed would depend on geometric properties of the self-assembling molecule and the thermodynamics of the self-aggregating process [37]. Considering both theoretically derived molecular geometries, compact-amphipathic or extended-zwitterionic, FB1 self-aggregating structures should be thought as either small micelles [38] or bilayers [39], respectively (Fig. 9a and b). Moreover, the value of FB1s c.m.c. determined was within the order of magnitude of micelle forming compounds (e.g. detergents) and far from that of bilayers forming phospholipids. Taken together these data and even though the extended structure might be the most probable conformation acquired by FB1 monomers in water [34] at concentrations below the c.m.c. (1.97 mM), a micellar structure may be proposed through a folding change driven by the hydrophobic effect upon FB1 self-aggregation. A similar folding change can also be considered upon FB1 binding to a membrane–water interface (see below).

4.2. FB1 binding and location at the membrane–water interface

Steady-state fluorescence anisotropy provides information about the organization of the membrane environment around the fluorescent probe. DPH is known to be located within the hydrocarbon chain region of the membrane core and its parent compound, TMA-DPH, stabilizes its DPH moiety at the polar head group region of bilayers [40]. FB1 significantly reduced, in a concentration-dependent manner, the molecular order and mobility at the bilayer membrane surface as revealed by the reduction in the anisotropy of TMA-DPH without affecting the dynamics at the hydrocarbon chain region demonstrated by the constancy in the anisotropy of DPH (Fig. 3). Taken together, the present results demonstrated the interfacial location of FB1. Hence the molecular mechanism of FB1 would involve a disruption of the structured water network at the lipid–water interface. Calorimetric studies would support this interpretation in the case that FB1 affected only the pre-transition $P_{\beta'} \rightarrow L_{\beta'}$ and not the main phase transition $L_{\beta'} \rightarrow L_{\alpha}$ of dpPC.

4.3. Characteristics of the initial membrane state that controls the toxin–membrane interaction

The monolayer π changes induced by FB1 were dependent on the subphase FB1 concentration and pH (Fig. 4) as well as on the monolayer's molecular packing (Fig. 4f) and surface charge (Fig. 5).

Surface pressure changes may be interpreted either as a toxin penetration in the monolayer and/or an interfacial deformation accompanying the toxin adsorption. The whole process of drug transference toward the monolayer is the sum of two contributions: (a) the change in the interactions of the solute with its surroundings, reflecting the change in the chemical microenvironment of the solute and (b) the work required to create a

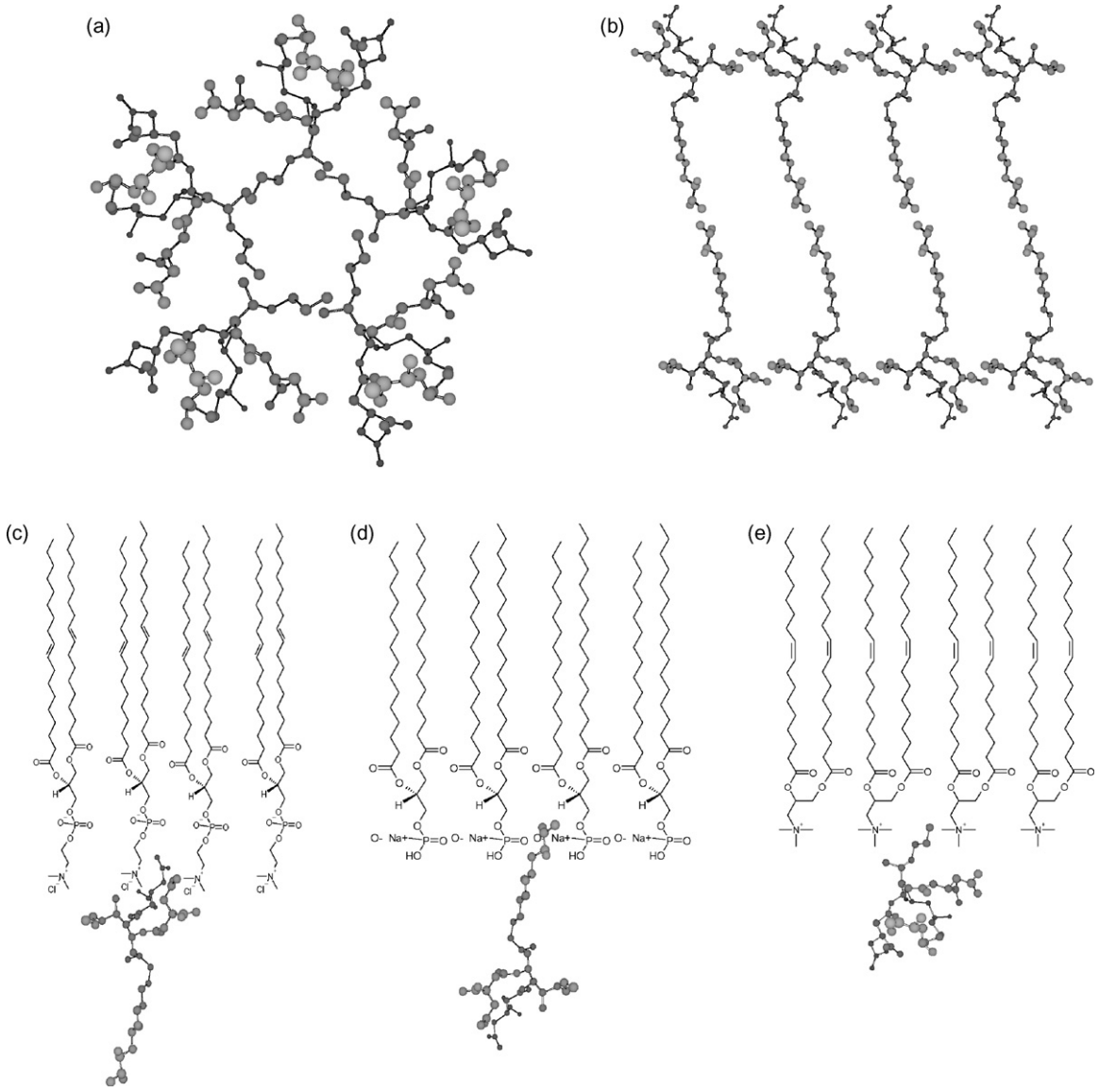

Fig. 9. Proposed models for the formation of FB1 self-aggregating structures (a and b), and for its interaction with dpPC (c), dpPC:dpPA (d), and dpPC:DOTAP (e) monomolecular layers.

cavity to incorporate the solute in-between the lipids, which can be described as a pressure–area-type work (W). The enhancement of the probability of cavity formation due to an increase in the surface molecular density is larger for the larger solutes [41].

According to this rationale, the FB1's binding kinetics and affinity (Fig. 4e) were higher than those of drugs having a smaller size and a more rigid structure such as promethazine, hydroxyzine and thioridazine [29]. Moreover, the higher molecular size that is expected for the deprotonated form of FB1 at low pH may explain the fact that the extent of the monolayer deformation ($\Delta\pi$) as well as the $\pi_{\text{cut-off}}$ of FB1 observed upon its penetration in a zwitterionic monolayer were higher at pH 2.63 than at pH 7 (Fig. 4f). In addition, the negative slope in the $\Delta\pi - \pi_i$ plot reflected the decreasing efficiency of the work of deformation done by FB1 against the increasing molecular cohesion forces of the monolayer (Fig. 4f).

4.3.1. *Effect of surface charge on FB1 binding*

The extent of interfacial deformation induced by FB1 upon its adsorption/penetration in the monolayer from the subphase was higher for charged interfaces if compared with a zwitterionic one, and the highest deformation was observed in the case of a positive monolayer (Fig. 5). Moreover, the monolayer's ΔV changed in the presence of FB1, increasing when it was mixed with dpPC or with dpPC–dpPA (Fig. 6a and b) and decreasing with dpPC–DOTAP (Fig. 6c).

To explain these results the FB1 conformations and folding changes described in Section 4.1 should be recalled. Assuming an extended conformation of FB1 (the most probably found in water), it can be suggested that this toxin was incorporated in the positive monolayer composed of dpPC–DOTAP through the carboxyl end which is more bulky than the positive amino terminus and that it may be more prone to face the negative dpPC–dpPA monolayer interface with the opposite orientation (Fig. 9c and d).

Different orientations were also suggested by the increase in the surface potential induced by FB1 in dpPC–dpPA mixed monolayer and its decrease in dpPC–DOTAP (Fig. 6b and c). This indicated that the negative end terminus of the FB1 molecular dipole component perpendicular to the monolayer plane pointed towards the water phase in the former and towards the air in the latter. In the case of the zwitterionic monolayer, the compact folding of FB1 may justify the lower monolayer deformation due to its incorporation through the hydrophobic end (lower cross sectional area) of the compact FB1 folding which left the carboxylic and the amino group containing chains grouped at the opposite end (Fig. 9e). This charge distribution in the zwitterionic type folding of FB1 would also induce a condensation within the polar region due to the intramolecular electrostatic attraction between positive ammonium and negative carboxyl groups. According to this rationale, the magnitude of the net molecular dipole may result more negative in the compact than in the extended conformation explaining the higher decrease in ΔV observed in dpPC if compared with dpPC–dpPA.

4.4. Effect of the molecular packing density on the FB1 ability to affect the monolayer structure and stability

Surface pressure–area isotherms provided information about FB1 stabilization in monolayers of different compositions. The effect of FB1 on the increase in the A_{min} of dpPC indicated that FB1 remained in the monolayer up to the π_c of the zwitterionic interface and its effect on increasing π_c suggested that it strengthens the molecular cohesion at high pressures perhaps through a stabilization of the interfacial water network (Fig. 6a). In monolayers of other compositions, FB1 induced an expansion only at low π without change neither π_c nor A_{min}. The constancy of π_c in the presence of FB1 in dpPC:DOTAP monolayers and its decrease in dpPC:dpPA suggested that, at collapse, the later mixture still contained FB1 whilst the former was free of it. Hence, FB1 was stable in negative monolayers up to higher surface pressures. The area expansion induced by FB1 in the isotherm at 35 mN/m followed the same magnitude order as that observed in penetration experiments (dpPC:DOTAP > dpPC:dpPA > dpPC). This is interesting because this π value (35 mN/m) may be considered as the equilibrium surface pressure of a bilayer [42].

The extent of monolayer deformation ($\Delta\pi$) will depend on the monolayer elasticity and the drug structural properties (size, shape and charge) and its upper limit will be determined either by the π_c of the pure lipid or by the drug–lipid mixture, provided the drug remains stable in the monolayer up to the collapse π. A monolayer destabilization would lead to a lost of molecular components through the collapse. These instabilities may be due to a curvature stress generated by the fact that molecules with high positive spontaneous curvature do not resist its confinement in a planar configuration at the air–water interface when π is too high. Moreover, the stronger the expansion the lower is the pressure at which FB1 is able to remain at the interface. This may be thought of as FB1 molecules, with a very high hydrophilic/hydrophobic relationship, inserted at the polar head group region of lipids and inducing a decrease in the molecular cohesion (hence stability) at the hydrocarbon chains region.

Epifluorescence studies revealed long-range effects of FB1 at the mesoscopic level (Fig. 7). The morphology of condensed lipid domains is essentially determined by the line tension at the domain boundary, the molecular chirality, dipolar repulsions between molecules and a large dipolar in-plane component that leads to domain growth in the direction of the molecular tilt [43]. FB1 effects on domain shapes should be interpreted in terms of its dipolar contribution and ability to disrupt the lipid molecular order and tilt orientation. In addition, our results demonstrate the different evolution of the domain shape depending on the imposed boundary conditions (e.g. initial π value, constant π or constant area) (Figs. 7 and 8). It is important to recall that the activity of lipolytic enzymes participating in signal transduction phenomena are dependent on the initial topological conditions and organization of their substrate which in turn are self-organized membrane components [18]. The initial membrane conditions will determine the final membrane state after FB1–membrane binding, and this in turn will be the initial conditions for the activities expression of mechanosensitive membrane proteins [44] and topology-dependent enzymes [18]. The FB1 toxicological activity will depend by this means on the membrane dynamics as well as on the membrane ability to relieve the mechanical tension elicited by the mycotoxin binding.

4.5. FB1 binding kinetics

FB1 exhibited a binding affinity for zwitterionic monolayers several orders of magnitude higher than many substances tested in our laboratory covering a wide range of chemical composition such as small hydrophobic drugs [29], a peptide [45] and a big protein [46]. This was mainly due to a high association rate accompanied by a very fast turnover and hence a high exchanging rate between the water and the membrane compartments. So, the resident time of FB1 at the membrane–water interface would be within the millisecond time scale. This is consistent with the small binding surface and low penetration capacity of the short hydrophobic tail of FB1 in the compact folding conformation which, according with the orientation suggested by our results shown in Fig. 4, would be facing the membrane.

5. Conclusions

The knowledge about modifications at the molecular level suffered by the organizational dynamics of biomembranes triggered by their direct interactions with FB1 at the early stages of this mycotoxin action mechanism is scarce. Hence, in the present work we evaluated the FB1 surface activity and membrane interactions.

We demonstrated the ability of FB1 to self-aggregate in water and to bind to membranes localizing at the polar head group region modifying the interface to an extent depending on the monolayer composition, the molecular packing and the subphase pH. We demonstrated the ability of FB1 to remain stable in model membranes packed even at the equilibrium π of bilayers and to modify the membrane molecular organization. Local interactions were transduced into long-range effects as shown by

changes in the shape of the lipid domains laterally self-separated in the model membrane studied. These FB1-induced effects on the membrane organization and dynamics would affect the general membrane properties that emerge at the supramolecular organizational level, e.g. the permeability as well as the activities of mechanosensitive integral proteins such as ion channels and topology-dependent lipolytic enzymes.

Highly remarkable were the evidences suggesting that FB1 adopted different orientations and/or foldings depending on the combined charge states of the toxin and the binding surface, as well as the demonstration that FB1 long-range effects depended on the boundary conditions. From the cellular perspective, the latter statement should be interpreted in terms of the cellular ability to relieve the tensions elicited by the mycotoxin binding.

Taken together, the present results support a lipid organization-mediated hypothesis of FB1 toxicity.

Acknowledgements

EMC is a graduate student from the Doctorado en Ciencias Biológicas, FCEFyN, UNC. This work was partially supported by grants form SeCyT-UNC, Agencia Nacional de Ciencia y Tecnología grant PICT2003 No 09-13801 and PICT2005 No 15-32256 and CONICET. MGT and EMC are fellowship holders and María A. Perillo is career investigator of the later institution.

References

[1] A.M. Calvo, R.A. Wilson, J.W. Bok, N.P. Keller, Microbiol. Mol. Biol. Rev. 66 (2002) 447.
[2] A.L. Demain, A. Fang, Adv. Biochem. Eng. Biotechnol. 69 (2000) 1.
[3] J.P. Rheeder, W.F. Marasas, H.F. Vismer, Appl. Environ. Microbiol. 68 (2002) 2101.
[4] W.C. Gelderblom, V. Sewram, G.S. Shephard, P.W. Snijman, K. Tenza, L. van der Westhuizen, R. Vleggaar, J. Agric. Food Chem. 55 (2007) 4388.
[5] P.E. Nelson, T.A. Toussoun, W.F.O. Marasas, *Fusarium* Species: An Illustrated Manual for Identification, Pennsylvania State University Press, University Park, PA, 1983.
[6] F.Q. Li, T. Yoshizawa, O. Kawamura, X.Y. Luo, Y.W. Li, J. Agric. Food Chem. 49 (2001) 4122.
[7] F.S. Chu, G.Y. Li, Appl. Environ. Microbiol. 60 (1994) 847.
[8] M.B. Doko, A. Visconti, Food Addit. Contam. 11 (1994) 433.
[9] E.T.P.G. Sydenham, W.F.O. Marasas, G.S. Shepard, D.J. Van Schalkwyk, K.R. Koch, J. Agric. Food Chem. 38 (1990) 1900.
[10] S.A. Missmer, L. Suarez, M. Felkner, E. Wang, A.H. Merrill Jr., K.J. Rothman, K.A. Hendricks, Environ. Health Perspect. 114 (2006) 237.
[11] G.S. Bondy, J.J. Pestka, J. Toxicol. Environ. Health B: Crit. Rev. 3 (2000) 109.
[12] M.G. Theumer, A.G. Lopez, D.T. Masih, S.N. Chulze, H.R. Rubinstein, Clin. Diagn. Lab. Immunol. 9 (2002) 149.
[13] L. Rumora, S. Kovacic, R. Rozgaj, I. Cepelak, S. Pepeljnjak, T. Zanic Grubisic, Arch. Toxicol. 76 (2002) 55.
[14] A.M. Domijan, D. Zeljezic, N. Kopjar, M. Peraica, Toxicology 222 (2006) 53.
[15] J.J. Yin, M.J. Smith, R.M. Eppley, S.W. Page, J.A. Sphon, Biochim. Biophys. Acta 1371 (1998) 134.
[16] IPCS-WHO, in: International Programme on Chemical Safety (Ed.), Fumonisin B1. Environmental Health Criteria, vol. 219, World Health Organization, Geneva, 2000.
[17] B. Vallee, H. Riezman, EMBO J. 24 (2005) 730.
[18] L. De Tullio, B. Maggio, S. Hartel, J. Jara, M.L. Fanani, Cell Biochem. Biophys. 47 (2007) 169.
[19] M.A. Perillo, R.K. Yu, B. Maggio, Biochim. Biophys. Acta 1193 (1994) 155.
[20] M.L. Fanani, S. Hartel, R.G. Oliveira, B. Maggio, Biophys. J. 83 (2002) 3416.
[21] J.M. Soriano, L. Gonzalez, A.I. Catala, Prog. Lipid Res. 44 (2005) 345.
[22] H.M. Burger, S. Abel, P.W. Snijman, S. Swanevelder, W.C. Gelderblom, Lipids 42 (2007) 249.
[23] E.A. Martinova, Biochemistry (Mosc.) 63 (1998) 102.
[24] M.C. Ferrante, R. Meli, G. Mattace Raso, E. Esposito, L. Severino, G. Di Carlo, A. Lucisano, Toxicol. Lett. 129 (2002) 181.
[25] J.J. Yin, M.J. Smith, R.M. Eppley, A.L. Troy, S.W. Page, J.A. Sphon, Arch. Biochem. Biophys. 335 (1996) 13.
[26] J.M. Sanchez, V.T.A. Del, M.A. Perillo, J. Photochem. Photobiol. B 89 (2007) 56.
[27] A.V. Turina, M.V. Nolan, J.A. Zygadlo, M.A. Perillo, Biophys. Chem. 122 (2006) 101.
[28] A.V. Turina, M.A. Perillo, Biochim. Biophys. Acta 1616 (2003) 112.
[29] L. de Matos Alves Pinto, S.V. Malheiros, A.C. Lino, E. de Paula, M.A. Perillo, Biophys. Chem. 119 (2006) 247.
[30] G.S. Shephard, E.W. Sydenham, P.G. Thiel, W.C.A. Gelderblom, J. Liquid Chromatogr 13 (1990) 2077.
[31] D.A. Garcia, M.A. Perillo, Biophys. Chem. 95 (2002) 157.
[32] F. Bordi, C. Cametti, A. Motta, M. Diociaiuti, A. Molinari, Bioelectrochem. Bioenerg. 49 (1999) 51.
[33] J.R. Lakowicz, Principles of Fluorescence Spectroscopy, Plenum Press, New York, 1983.
[34] F.A. Momany, M.A. Dombrink-Kurtzman, J. Agric. Food Chem. 49 (2001) 1056.
[35] R.C. Beier, M.H. Elissalde, L.H. Stanker, Bull. Environ. Contam. Toxicol. 54 (1995) 479.
[36] R.C. Beier, L.H. Stanker, Arch. Environ. Contam. Toxicol. 33 (1997) 1.
[37] M.A. Perillo, N.J. Scarsdale, R.K. Yu, B. Maggio, Proc. Natl. Acad. Sci. U.S.A. 91 (1994) 10019.
[38] J.N. Israelachvili, Intermolecular and Surface Forces, Academic Press, New York, 1989.
[39] T. Benvegnu, M. Brard, D. Plusquellec, Curr. Opin. Colloid Interf. Sci. 8 (2004) 469.
[40] F.G. Prendergast, R.P. Haugland, P.J. Callahan, Biochemistry (Mosc) 20 (1981) 7333.
[41] S. Mitragotri, M.E. Johnson, D. Blankschtein, R. Langer, Biophys. J. 77 (1999) 1268.
[42] D. Marsh, Biochim. Biophys. Acta 1286 (1996) 183.
[43] K. Thirumoorthy, N. Nandi, D. Vollhardt, Langmuir 23 (2007) 6991.
[44] O.P. Hamill, B. Martinac, Physiol. Rev. 81 (2001) 685.
[45] M.E. Sanchez-Borzone, M.E. Cobe, M.A. Perillo, Abstracts book, in: Proceedings of the XXXVI Annual Meeting of the Argentinean Biophysical Society, International Conference of Biological Physics, Southern Cone Biophysics Congress, 2007, p. 122.
[46] E.M. Clop, J.M. Sánchez, M.A. Perillo, Abstracts book, in: Proceedings of the XXXI Annual Meeting of the Biophysics Society of Argentina, 2002, p. 110.